


# Analogous seasonal evolution of the South Atlantic SST dipole indices

Hyacinth C. Nnamchi,<sup>1,\*†</sup>  Fred Kucharski,<sup>2,3</sup> Noel S. Keenlyside<sup>4,5</sup> and Riccardo Farneti<sup>2</sup><sup>1</sup>Department of Geography, University of Nigeria, Nsukka, Nigeria<sup>2</sup>Earth System Physics Section, The Abdus Salam International Centre for Theoretical Physics, Trieste, Italy<sup>3</sup>Center of Excellence for Climate Change Research/Department of Meteorology, King Abdulaziz University, Jeddah, Saudi Arabia<sup>4</sup>Geophysical Institute, University of Bergen, Norway<sup>5</sup>Bjerknes Centre for Climate Research, Bergen, Norway

\*Correspondence to:

H. C. Nnamchi, Department of  
Geography, University of Nigeria,  
Nsukka 410001, Nigeria.

E-mail:

[hyacinth.nnamchi@unn.edu.ng](mailto:hyacinth.nnamchi@unn.edu.ng)

†Current address:

GEOMAR|Helmholtz Centre for  
Ocean Research Kiel,

Düsterbrookweg 20,

24105 Kiel, Germany.

E-mail: [hnnamchi@geomar.de](mailto:hnnamchi@geomar.de)

## Abstract

**Two variants of sea-surface temperature (SST) dipole indices for the South Atlantic Ocean (SAO) has been previously described representing: (1) the South Atlantic subtropical dipole (SASD) supposedly peaking in austral summer and (2) the SAO dipole (SAOD) in winter. In this study, we present the analysis of observational data sets (1985–2014) showing the SASD and SAOD as largely constituting the same mode of ocean–atmosphere interaction reminiscent of the SAOD structure peaking in winter. Indeed, winter is the only season in which the inverse correlation between the northern and southern poles of both indices is statistically significant. The observed SASD and SAOD indices exhibit robust correlations ( $P \leq 0.001$ ) in all seasons and these are reproduced by 54 of the 63 different models of the Coupled Models Intercomparison Project analysed. Their robust correlations notwithstanding the SASD and SAOD indices appear to better capture different aspects of SAO climate variability and teleconnections.**

**Keywords:** SST dipole; seasonal evolution; CMIP3/5; South Atlantic OceanReceived: 16 March 2017  
Revised: 1 July 2017  
Accepted: 4 September 2017

## 1. Introduction

A dipole structure in sea-surface temperature (SST) anomalies represents the dominant mode of ocean–atmosphere fluctuations in the South Atlantic. The origins of the dipole has been attributed to the interactions of the ocean mixed layer with atmospheric fluctuations via surface heat fluxes (Fauchereau *et al.*, 2003; Sterl and Hazeleger, 2003; Trzaska *et al.*, 2007; Morioka *et al.*, 2011; Nnamchi *et al.*, 2016). The dipole structure is typically oriented in the southwest–northeast direction, and two major variants have been described in the literature – the South Atlantic subtropical dipole (SASD) and the South Atlantic Ocean (SAO) dipole (SAOD).

The monthly standard deviation of the SASD index peaks in austral summer when the SAO mixed layer depth is shallowest (Morioka *et al.*, 2011). The SASD is considered as a subtropical mode, with the northernmost part at  $\sim 15^\circ$ – $25^\circ$ S. However, the empirical orthogonal function (EOF) analysis of seasonally stratified data sets also shows opposite structure of SST anomalies between the equatorial and southwest Atlantic peaking in austral winter (Nnamchi *et al.*, 2011). This dipole pattern is referred to as the SAOD. While the northernmost part of the SAOD extends to the equator and coincides with the Atlantic Niño (ATL3) in both space and time, leading to the notion that the two may represent the same mode of variability (Nnamchi

*et al.*, 2016); by definition, the southern part of the SASD ( $30^\circ$ N– $40^\circ$ S,  $10^\circ$ – $30^\circ$ W) falls within that of the SAOD ( $25^\circ$ N– $40^\circ$ S,  $10^\circ$ – $40^\circ$ W).

Are SASD and SAOD related or independent modes of ocean–atmosphere variability? To illustrate this question, Figure S1, Supporting Information, shows the first EOF mode of monthly SST anomalies over the SAO; characterised by a dipole associated with a basin-scale cyclonic atmospheric anomalies. There are broad cold anomalies in the southern arms of the SASD and SAOD as well as in the subtropical and equatorial warming peaks leading to SASD and SAOD definitions, respectively. The associated time series displays interannual-to-decadal fluctuations (Venegas *et al.*, 1997; Trzaska *et al.*, 2007; Nnamchi *et al.*, 2016) with robust correlations with the ATL3, SASD, and SAOD indices ( $P < 0.001$ ) as shown in Table S1. The SAOD has similarly significant correlations with the ATL3 and SASD indices ( $r \sim 0.70$ ). The ATL3|SAOD correlation has been described elsewhere (Nnamchi *et al.*, 2016) but that of the SASD and SAOD remains unclear and is therefore the focus of the present study.

## 2. Data and methods

Using satellite-derived SST data set on  $1.0^\circ \times 1.0^\circ$  latitude–longitude horizontal grids (Reynolds *et al.*, 2007) and satellite-era atmospheric reanalysis on

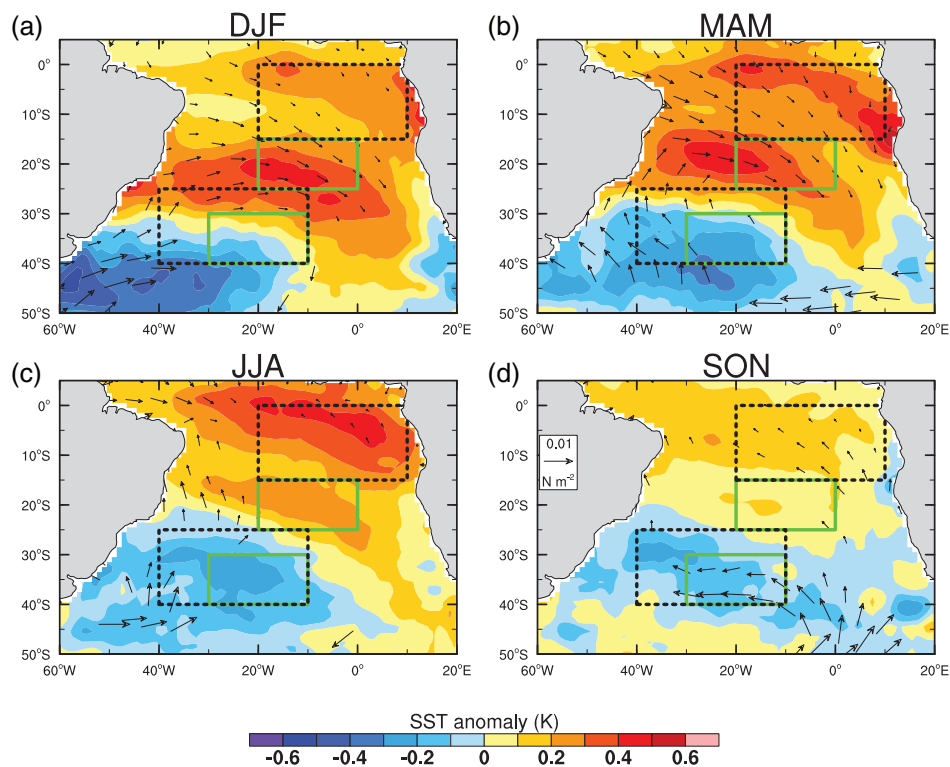


**Figure 1.** Spatial patterns of the leading S-EOF mode of DJF to SON SST anomalies over the SAO during 1985–2014. Arrows show statistically significant wind stress anomalies at 95% confidence level.

$2.5^\circ \times 2.5^\circ$  grids (Kanamitsu *et al.*, 2002), we analysed the 30-year period from 1985 to 2014 with generally improved observations. We first created SST anomaly by subtracting the mean annual cycle from the original data set and then calculated the deviations from the global-mean warming trend as follows:

$$\text{SSTA}'_{x,y,t} = \text{SSTA}_{x,y,t} - \beta_t$$

where the subscripts ( $x, y, t$ ) represent the zonal and meridional directions and time;  $\text{SSTA}'$  denotes the deviations of the SST anomaly (SSTA) at every grid point ( $x, y$ ) from the least-squares linear trend coefficient of the global-mean ( $\beta$ ). Other variables were linearly detrended at every grid point using the least-squares method. All statistical significance tests are based on two-tailed  $t$ -test. The warm and cold anomalies of the leading dipole are confined between  $5^\circ\text{N}$  and  $50^\circ\text{S}$  (Figure S1(a)) and this meridional extent is used for subsequent analyses.

### 3. Analyses and results

#### 3.1. Seasonal evolution of the interannual SST dipole

Patterns of SST anomalies such as dipole in the SAO primarily represent fluctuations above and below the mean annual cycle in different seasons of the year. Different parts of the equatorial and SAO display marked annual cycle of SST that often exceed the interannual anomalies in amplitude (Burls *et al.*, 2011;

Nnamchi *et al.*, 2016). Thus, the SST anomalies may be strongly modulated by the climatological-mean annual cycles, which denote the background conditions under which the ocean–atmosphere fluctuations evolve. Here, we investigate the seasonal evolution of the dominant dipole mode of SAO SST anomalies using the seasonal-reliant EOF (S-EOF) analysis (Wang and An, 2005). We define a four-season sequence that spans from the austral summer of a year denoted as D(–1) JF(0) to the following spring [September–October–November (SON)] denoted as SON(0). To construct the covariance matrix, the SST anomalies in each seasonal sequence are treated as an integral block [of one time step for the year (0)]. The EOF decomposition is then performed and the expansion coefficient (EC) time series derived for each eigenvector that contains a sequence of four seasonally evolving SST pattern maps from D(–1)JF(0) to SON(0). The major advantage of S-EOF analysis over the conventional method is that the four seasonal maps are directly related to the yearly EC time series and depict the overall seasonal evolution.

The leading S-EOF mode is characterised by the evolution of a meridional dipole structure in SST anomalies over the SAO during the course of the seasons (Figure 1). In DJF, the cold anomalies are mainly confined to the regions around latitude  $35^\circ\text{S}$  and further south; the rest of the basin is characterised by warm anomalies. Localised bands of anomalous warm maxima are observed close to the northern pole of the SASD and in the Benguela–equatorial Niño region. The subtropical pattern does not really fit the SASD definition:

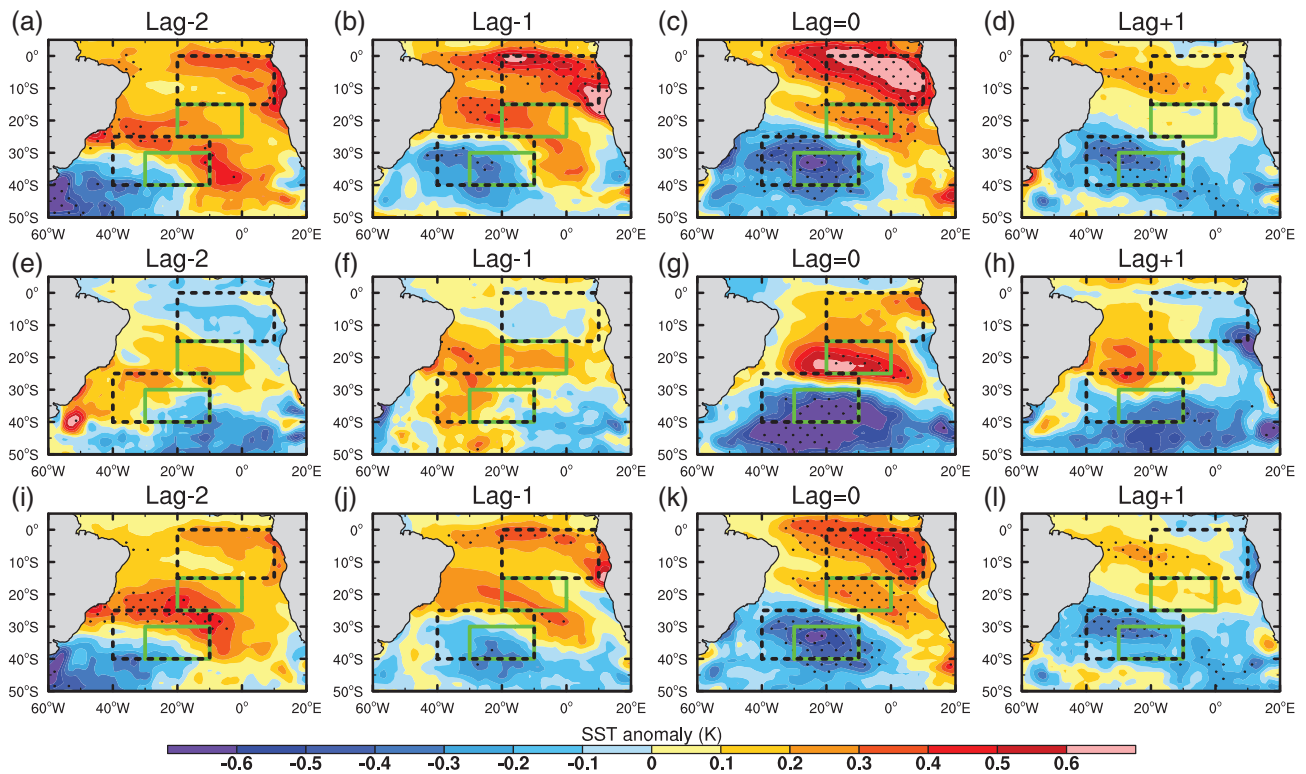


**Figure 2.** Composite evolution of the SAOD (a–d) and SASD (e–h) SST anomalies. The maps are based on the ( $\pm 1.0\sigma$ ) composite difference using the SAOD (SASD) index for JJA (DJF) as lag = 0. The lower panels (i–l) are based on SASD index with JJA as lag = 0. Stipples denote a statistical significance at  $P \leq 0.05$ . The pattern correlations between the corresponding in panels (a–d) and (i–l) are 0.93, 0.88, 0.96, and 0.92 for DJF, MAM, JJA, and SON, respectively.

the cold anomalies are displaced to the west of the SASD box while both the cold and warm anomalies are displaced south by the order of  $\sim 5^\circ - 10^\circ$  of latitude. There are widespread robust wind anomalies suggestive of atmospheric-induced origin of the SST anomalies (Venegas *et al.*, 1997; Sterl and Hazeleger, 2003; Hermes and Reason, 2005) and this pattern tends to lead a similar dipole structure in subtropical Indian Ocean by 1 month (Hermes and Reason, 2005). In the equatorial region, there is a weak Niño-like structure probably reflecting the type II ATL3 described by Okumura and Xie (2006) or an early phase of the Benguela Niño.

In MAM, the SST and wind stress anomalies spread northward such that the cold anomalies reach  $\sim 30^\circ\text{S}$  (Figure 1(b)). The cyclonic wind stress anomalies intensify and are associated with enhanced warming anomalies from the northern part of the SASD to the Benguela–equatorial Niño region. This season marks the peak phase of the Benguela Niño and the large-scale cyclonic wind stress anomalies appear as northwesterly perturbations originating from the equatorial region (Florenchie *et al.*, 2003, 2004). Nonetheless, the sequence of the wind stress anomalies from DJF to MAM points to important roles for atmospheric anomalies in the southwest subtropics and extratropics.

By JJA, the dipole structure advances further north (Figure 1(c)); the cold anomalies reach  $\sim 20^\circ\text{S}$  with the result that the centre of maximum cold anomalies clearly fit into the southern poles of both the SASD and SAOD. Further north, the Benguela Niño weakens

giving rise to a more zonal structure of warming characteristic of the Atlantic Niño. Compared to MAM, the wind stress anomalies are generally weaker in JJA consistent with previous studies suggesting that peak in wind fluctuations precedes that of SST anomalies (Keenlyside and Latif, 2007; Richter *et al.*, 2013). While the westerly anomalies persist over the western equatorial Atlantic, a reversal (to easterlies) occurs in the eastern basin leading to anomalous convergent motion over the equatorial ATL3 region:  $0^\circ - 20^\circ\text{W}$ . Thus, the SST and related wind stress anomalies in JJA may be driven ocean dynamics consistent with the heat budget calculations of Nnamchi *et al.*, (2016). The anomalous easterlies intensify further indicating a strengthening of the trade winds (Figure 1(d)). This may then intensify upwelling and evaporation leading to the decay of the SST anomalies.

### 3.2. Seasonal variability and correlations of the dipole SST indices with other climate modes

Here, we investigate how well the SST anomalies depicted in Figure 1 could be reproduced using composite difference based on a unit standard deviation ( $\pm 1.0\sigma$ ) of the SASD and then SAOD index. For the SASD (SAOD), season (0) is DJF (JJA) on the basis of previous studies suggesting that the patterns peak in these seasons (Morioka *et al.*, 2011; Nnamchi *et al.*, 2011). The composite maps are then lagged in time for the two preceding and one following season. The

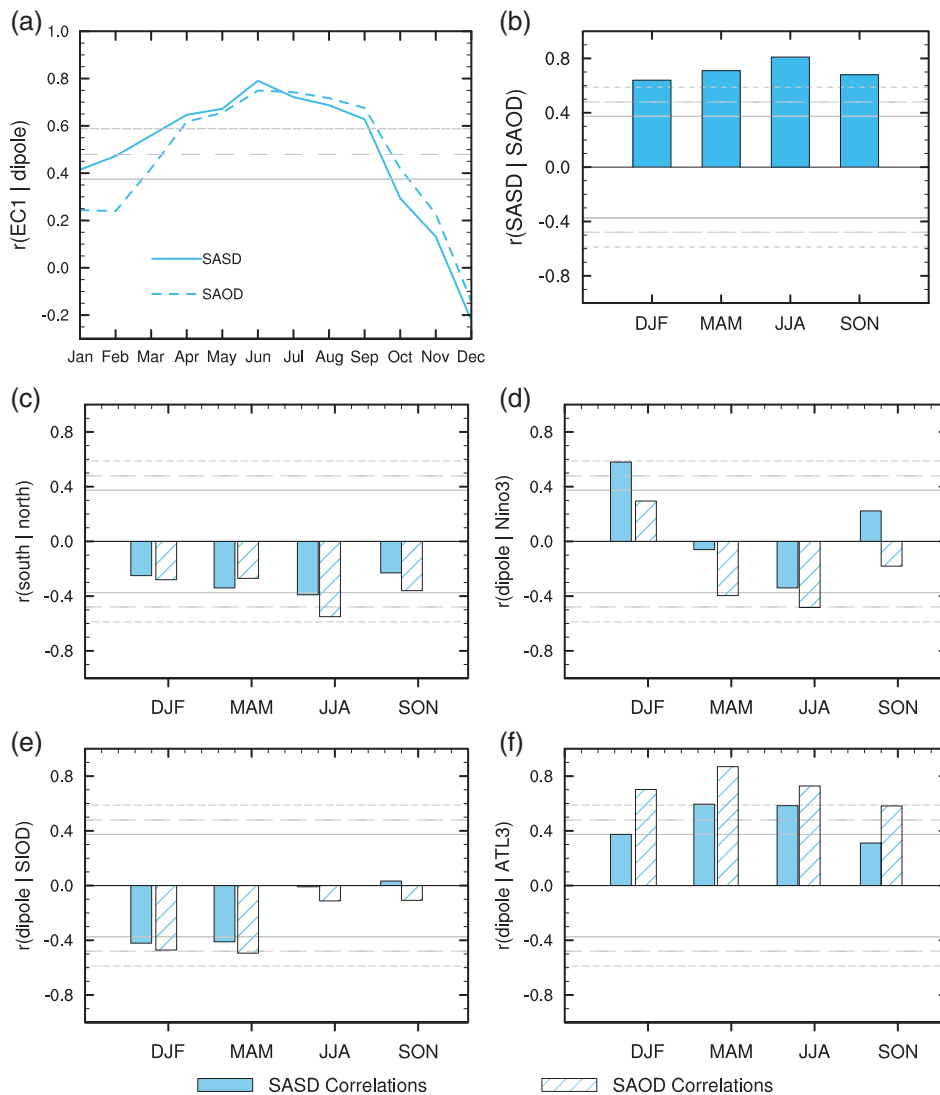


**Figure 3.** (a) Correlations of the leading S-EOF mode EC time series of SAO SST anomalies with SST-based indices of dipole. (b) Coefficients of correlation between the SASD and SAOD indices and (c) between their northern and southern poles. (d–f) Correlations of the SASD and SAOD indices with Niño-3, SIOD, and ATL3. In all panels, solid ( $P = 0.05$ ); long-dashed ( $P = 0.01$ ); and short-dashed ( $P = 0.001$ ) grey lines denote statistical significance levels. The Niño-3 is defined as SST anomalies averaged in the region  $5^{\circ}\text{N}–5^{\circ}\text{S}$ ,  $90^{\circ}–150^{\circ}\text{W}$  and the SIOD as the difference between averages over ( $30^{\circ}–44^{\circ}\text{S}$ ,  $74^{\circ}–44^{\circ}\text{E}$ ) and ( $19^{\circ}–35^{\circ}\text{S}$ ,  $80^{\circ}–110^{\circ}\text{E}$ ).

results show robust opposite SST anomalies over the SAO at lag-2, which intensify further at lag-1 leading to the peak phase of the SAOD similar to the S-EOF patterns (Figures 2(a)–(d)). However, such progressive evolution is not found for the SASD (Figures 2(e)–(h)); rather, the SST dipole anomalies are robust only at lag=0. It is not surprising therefore that the DJF SASD and JJA SAOD time series are not correlated ( $r = 0.07$ ), consistent with the event-based analysis which shows that the  $\pm 1.0\sigma$  SST anomalies do not tend to occur in the same year (Table S2). On the other hand, if JJA is used as season (0), the SASD-related anomalies evolve in a fashion analogous to the SAOD (Figures 2(i)–(l)) with spatial correlations in the range of  $0.88 \geq r \leq 0.96$ .

We further investigate the similarity in temporal evolution of the SASD and SAOD by calculating their month-by-month correlations with EC1 (which

has a constant value for each year; Figure 3(a)). Both correlation curves increase progressively from January, peak in June, and then declines during the remaining months of the year. The SASD curve notably exceeds that of the SAOD curve in the first 3 months, but the two curves converge as from April and by peaking in austral winter seem to describe the SAOD. The SASD and SAOD indices are significantly correlated at  $P < 0.001$  in all seasons with a peak in JJA (Figure 3(b)). As a direct measure of the polarity of these dipole indices, the inverse correlation between their southern and northern poles also peak in JJA (Figure 3(c)). Indeed, JJA is the only season for which the correlation is statistically significant for both indices; although the anticorrelation is stronger for the SAOD ( $P < 0.01$ ) than the SASD ( $P < 0.05$ ). The highest absolute correlations in JJA in all panels of Figures 3(a)–(c) appear to confirm the occurrence of the SST dipole peak in this season.



**Figure 4.** Coefficients of correlation between the SASD and SAOD indices simulated by the CMIP3 and CMIP5 models. The numbers 1, 2, 3, and 4 correspond to DJF, MAM, JJA, and SON, respectively. The panels are arranged in alphabetical order of model names: CMIP3 in lower case and CMIP5 in upper case letters. In all panels, solid ( $P = 0.05$ ); long-dashed ( $P = 0.01$ ); and short-dashed ( $P = 0.001$ ) lines denote statistical significance levels.

Previous studies show that the SAO SST dipole may be related to the Pacific El Niño (Rodrigues *et al.*, 2015), the subtropical Indian Ocean dipole (SIOD) (Hermes and Reason, 2005) and Atlantic Niño (Nnamchi *et al.*, 2016). Here, indices representing these climate modes are correlated with those of the SASD and SAOD for comparison. The SASD (SAOD) index is better correlated with the Niño-3 index in DJF (MAM and JJA) and these seasons depict different phases of El Niño–SAO dipole correlations (Figure 3(d)). The dipole is related to the SIOD in DJF and MAM and to the ATL3 in all seasons; in both cases, the SAOD index exhibits stronger correlations (Figures 3(e) and (f)).

### 3.3. Representation in coupled climate models

We have so far shown robust correlations between the SASD- and SAOD-related anomalies in space and time.

It is then necessary to understand whether the current generation of state-of-the-art coupled models are able to reproduce these observed correlations or not. Thus, we analysed the SST simulated by 63 different numerical models of the Coupled Models Intercomparison Project phases 3 and 5 (CMIP3/5) (Meehl *et al.*, 2007; Taylor *et al.*, 2012). This represents the ‘climate of the 20th-century’ experiment of the available 23 CMIP3 ([http://www-pcmdi.llnl.gov/ipcc/data\\_status\\_tables.htm](http://www-pcmdi.llnl.gov/ipcc/data_status_tables.htm)) and the 40 CMIP5 (<http://cmip-pcmdi.llnl.gov/cmip5/availability.html>) models providing first realisation of the ‘historical’ experiment. The modelled SSTs were bilinearly remapped to a common  $1.0^\circ \times 1.0^\circ$  longitude–latitude horizontal grids for comparison with observational data set (Rayner *et al.*, 2003) and both were linearly detrended for the last 30 years available for all models during 1970–1999.

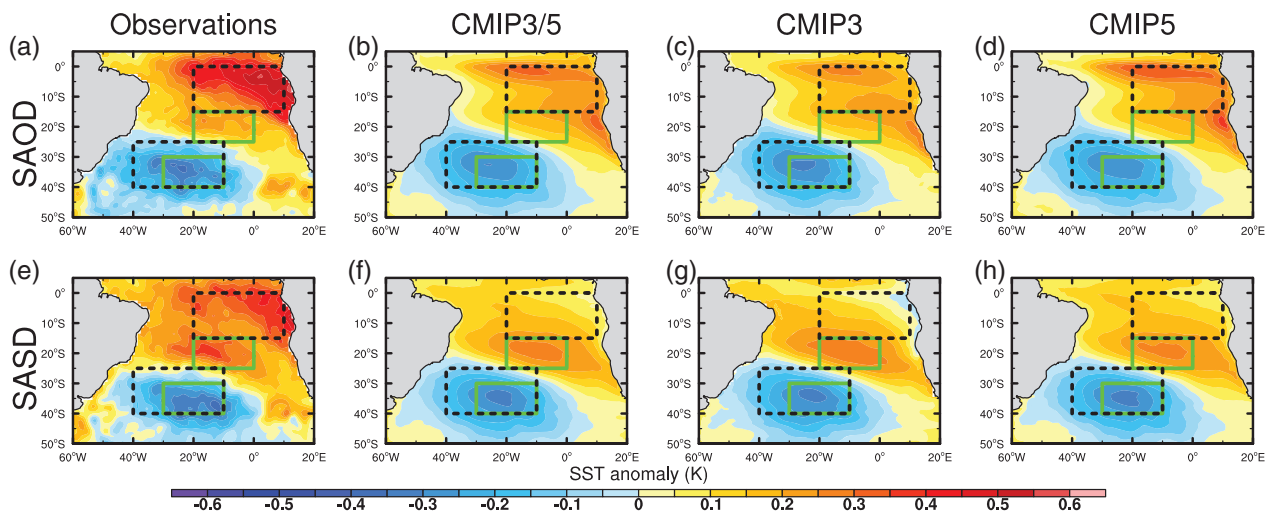


**Figure 5.** Upper panel: SST anomalies regressed on the SAOD index for JJA based on (a) observational data set, (b) CMIP3/5 multimodel mean, (c) CMIP3 multimodel mean, and (d) CMIP5 multimodel mean. (e–h) Similar to (a–d) but for the SST anomalies regressed SASD index for JJA.

The seasonality of SASDISAOD correlation may be nonstationary in time as the JJA peak during the 1984–2014 (Figure 3(b)) period is not reproduced during 1970–1999, although the correlations remain robust in all seasons (Figure 4). Consistent with observations, all the CMIP3/5 models simulated positive correlation between the SASD and SAOD indices in all seasons. At  $P \leq 0.001$ , these correlations are statistically significant in 54 of the 63 models in all four seasons; 58 models in at least three seasons and 59 models in at least two seasons – suggesting that the CMIP3/5 models are able to reproduce the observed robust correlation between the SASD and SAOD indices. We further examined the spatial distribution of the SST anomalies associated with the SASD and SAOD indices in the CMIP3/5 models focusing on JJA during which the dipole has been shown to peak (Figure 5). The maps were constructed by regressing SST anomalies onto the dipole indices for each model and then the multimodel mean calculated for comparison with observations.

Figures 5(a) and (e) show similar dipole SST response to both indices with a pattern correlation of 0.94 in observations. The SASD and SAOD indices correctly reproduce cold anomalies over southwest Atlantic Ocean in the CMIP3/5 models. On the other hand, while the simulated SAOD index is also able to reproduce the broad features of the northern warm anomalies (Figure 5(b)), the SASD shows weak anomalies over the Benguela–equatorial Niño region (Figure 5(f)). The CMIP5 models show overall improvements in the simulation of the SASD compared to CMIP3 – the pattern correlation with observational data set changes from 0.71 to 0.80 but the SAOD pattern remains largely unchanged.

#### 4. Summary and discussions

A comparative analysis of the SASD and SAOD indices using observational data sets (1985–2014) shows a

peak during the austral winter consistent with the SAOD definition. Either the SASD or SAOD index may be used to represent the dipole mode: the two indices yield closely matched patterns with spatial correlations of seasonally stratified composite maps in the range of 0.88–0.96. The indices are equally strongly correlated in time in all seasons ( $P < 0.001$ ). However, the SAOD index seems to have stronger polarity and more robust correlations with SIOD and ATL3. Nonetheless, the peak phase of El Niño in DJF is correlated with SASD and it may therefore be more useful for characterising El Niño teleconnections with the SAO in this season. On the other hand, El Niño is correlated with the SAOD in MAM and JJA.

Warm and cold events of the cold tongue tend to occur on a large-scale encompassing the Benguela and equatorial Niño regions (Florenchie *et al.*, 2004; Lübbecke *et al.*, 2010; Lutz *et al.*, 2013). Whereas previous studies linked the origins of this broad warming to equatorial northwesterly atmospheric fluctuations, our results suggest important roles for wind stress anomalies in the southwest SAO subtropics and extratropics starting from the austral summer. The wind anomalies are underlain by opposite phase in SST giving rise to an emerging dipole structure (Colberg and Reason, 2007; Nnamchi *et al.*, 2011, 2016). The dipole evolves progressively and appears to propagate northward during the subsequent months with a peak phase in winter consistent with the seasonality of Atlantic Niño.

The present day generation of coupled models appear to be capable of reproducing the observed robust correlation between the SASD and SAOD indices: 54 of the 63 different CMIP3/5 models analysed have significant coefficients at  $P < 0.001$  in all seasons. However, the multimodel mean SST anomalies associated with the SAOD index better represents the observed amplitudes in the Benguela–equatorial Niño region, often considered vital for climate fluctuations over tropical Atlantic and further afield (Losada *et al.*, 2012; Syed

and Kucharski, 2016; Kucharski and Joshi, 2017). Nonetheless, the subtropical SAO variability represented by the SASD affects climate variability in this region (Morioka *et al.*, 2011; Rodrigues *et al.*, 2015). Thus, our results suggest that despite robust correlation between the SASD and SAOD indices, each may better capture different aspects of SAO climate variability and teleconnections.

### Acknowledgements

HCN and NSK were supported by the EU FP7/2007–2013 PREFACE Project. HCN carried out parts of the study during research stay at the Abdus Salam International Centre for Theoretical Physics through the Associateship Scheme. NSK also acknowledges support from the Research Council of Norway (233680/E10).

### Supporting information

The following supporting information is available:

**Figure S1.** Leading EOF mode of SST anomalies (January 1985–December 2014) over the South Atlantic Ocean: 5°N–50°S, 20°E–60°W. Shown are the (a) spatial pattern and (b) EC time series. In panel (a), the associated variance is shown in the top right corner; solid green boxes (15°–25°S, 0°–20°W and 30°–40°S, 10°–30°W) indicate the SASD domains (Morioka *et al.*, 2011), the dashed black boxes (7°–15°S, 10°E–20°W and 25°–40°S, 10°–40°W) show the SAOD domains (Nnamchi *et al.*, 2011).

**Table S1.** Correlation of the monthly S-EOF EC1 with equatorial and southern Atlantic SST-based indices, 1985–2014.

**Table S2.** Years of occurrence of  $\pm 1.0\sigma$  of the SASD and SAOD indices, 1985–2014.

### References

- Burls NJ, Reason CJC, Penven P, Philander SG. 2011. Similarities between the tropical Atlantic seasonal cycle and ENSO: an energetics perspective. *Journal of Geophysical Research: Oceans* **116**: C11010. <https://doi.org/10.1029/2011JC007164>.
- Colberg F, Reason CJC. 2007. Ocean model diagnosis of low frequency climate variability in the South Atlantic. *Journal of Climate* **20**: 1016–1034.
- Fauchereau N, Trzaska S, Richard Y, Roucou P, Camberlin P. 2003. Sea-surface temperature co-variability in the southern Atlantic and Indian oceans and its connections with the atmospheric circulation in the southern hemisphere. *International Journal of Climatology* **23**: 663–677. <https://doi.org/10.1002/joc.905>.
- Florenchie P, Lutjeharms JRE, Reason CJC, Masson S, Rouault M. 2003. The source of Benguela Niños in the South Atlantic Ocean. *Geophysical Research Letters* **30**: 1505, 10. <https://doi.org/10.1029/2003GL017172>.
- Florenchie P, Reason CJC, Lutjeharms JRE, Rouault M, Roy C, Masson S. 2004. Evolution of interannual warm and cold events in the southeast Atlantic Ocean. *Journal of Climate* **17**: 2318–2334.
- Hermes JC, Reason CJ. 2005. Ocean model diagnosis of interannual coevolving SST variability in the south Indian and South Atlantic oceans. *Journal of Climate* **18**: 2864–2882.
- Kanamitsu M, Ebisuzaki W, Woollen J, Yang S, Hnilo J, Fiorino M, Potter G. 2002. NCEP–DOE AMIP-II reanalysis (R-2). *Bulletin of the American Meteorological Society* **83**: 1631–1643. <https://doi.org/10.1175/BAMS-83-11-1631>.
- Keenlyside NS, Latif M. 2007. Understanding Equatorial Atlantic Interannual Variability. *Journal of Climate* **20**: 131–142.
- Kucharski F, Joshi MK. 2017. Influence of tropical South Atlantic sea surface temperatures on the Indian summer monsoon in CMIP5 models. *Quarterly Journal of the Royal Meteorological Society* **143**: 1351–1363.
- Losada T, Rodríguez-Fonseca B, Kucharski F. 2012. Tropical influence on the summer Mediterranean climate. *Atmospheric Science Letters* **13**: 36–42.
- Lübbecke JF, Böning CW, Keenlyside NS, Xie S-P. 2010. On the connection between Benguela and equatorial Atlantic Niños and the role of the South Atlantic anticyclone. *Journal of Geophysical Research – Atmospheres* **115**: C09015. <https://doi.org/10.1029/2009JC005964>.
- Lutz K, Rathmann J, Jacobeit J. 2013. Classification of warm and cold water events in the eastern tropical Atlantic Ocean. *Atmospheric Science Letters* **14**: 102–106.
- Meehl GA, Covey C, Delworth T, Latif M, McAvaney B, Mitchell JFB, Stouffer RJ, Taylor KE. 2007. The WCRP CMIP3 multi-model dataset: a new era in climate change research. *Bulletin of the American Meteorological Society* **88**: 1383–1394.
- Morioka Y, Tozuka T, Yamagata T. 2011. On the growth and decay of the subtropical dipole mode in the South Atlantic. *Journal of Climate* **24**: 5538–5554.
- Nnamchi HC, Li J, Anyadike RNC. 2011. Does a dipole mode really exist in the South Atlantic Ocean? *Journal of Geophysical Research: Atmospheres* **116**: D15104. <https://doi.org/10.1029/2010JD015579>.
- Nnamchi HC, Li J, Kucharski F, Kang I-S, Keenlyside NS, Chang P, Farneti R. 2016. An equatorial–extratropical dipole structure of the Atlantic Niño. *Journal of Climate* **29**: 7295–7311.
- Okumura Y, Xie S-P. 2006. Some overlooked features of tropical Atlantic climate leading to a new Niño-like phenomenon. *Journal of Climate* **19**: 5859–5874.
- Rayner NA, Parker DE, Horton EB, Folland CK, Alexander LV, Rowell DP, Kent EC, Kaplan A. 2003. Global analyses of sea surface temperature, sea ice, and night marine air temperature since the late nineteenth century. *Journal of Geophysical Research-Atmospheres* **108**: 4407. <https://doi.org/10.1029/2002JD002670>.
- Reynolds RW, Smith TM, Liu C, Chelton DB, Casey KS, Schlax MG. 2007. Daily high-resolution-blended analyses for sea surface temperature. *Journal of Climate* **20**: 5473–5496.
- Richter I, Behera SK, Masumoto Y, Taguchi B, Sasaki H, Yamagata T. 2013. Multiple causes of interannual sea surface temperature variability in the equatorial Atlantic Ocean. *Nature Geoscience* **6**: 43–47.
- Sterl A, Hazeleger W. 2003. Coupled variability and air–sea interaction in the South Atlantic Ocean. *Climate Dynamics* **21**: 559–571.
- Rodrigues RR, Campos EJ, Haarsma R. 2015. The impact of ENSO on the South Atlantic subtropical dipole mode. *Journal of Climate* **28**: 2691–2705.
- Syed FS, Kucharski F. 2016. Statistically related coupled modes of south Asian summer monsoon interannual variability in the tropics. *Atmospheric Science Letters* **17**: 183–189.
- Taylor K, Stouffer R, Meehl G. 2012. An overview of CMIP5 and the experiment design. *Bulletin of the American Meteorological Society* **93**: 485–498.
- Trzaska S, Robertson AW, Farrara JD, Mechoso CR. 2007. South Atlantic variability arising from air–sea coupling: local mechanisms and tropical–subtropical interactions. *Journal of Climate* **20**: 3345–3365.
- Venegas S, Mysak L, Straub D. 1997. Atmosphere–ocean coupled variability in the South Atlantic. *Journal of Climate* **10**: 2904–2920.
- Wang B, An S-I. 2005. A method for detecting season-dependent modes of climate variability: S-EOF analysis. *Geophysical Research Letters* **32**: L15710. <https://doi.org/10.1029/2005GL022709>.